bioRxiv preprint doi: https://doi.org/10.1101/137943; this version posted May 14, 2017. The copyright holder for this preprint (which was not certified by peer review) is the author/funder, who has granted bioRxiv a license to display the preprint in perpetuity. It is made available under aCC-BY-NC 4.0 International license.

Uncovering the drivers of animal-host microbiotas with joint distribution modeling

Johannes R. Björk[1,4*], Francis KC. Hui[2], Robert B. O'Hara[3], and Jose M. Montoya[4]

[1]Department of Biological Sciences, University of Notre Dame, United States

[2]Mathematical Sciences Institute, The Australian National University, Canberra, Australia

[3]Department of Mathematical Sciences, NTNU, Trondheim, Norway

[3]Biodiversity and Climate Research Centre, Frankfurt, Germany

[4]Theoretical and Experimental Ecology Station, CNRS-University Paul Sabatier, Moulis, France

[1,4*]*rbjork@nd.edu (Corresponding author)*

[2]*francis.hui@anu.edu.au*

[3]*bob.ohara@ntnu.no*

[4]*josemaria.montoyateran@sete.cnrs.fr*

May 15, 2017

bioRxiv preprint doi: https://doi.org/10.1101/137943; this version posted May 14, 2017. The copyright holder for this preprint (which was not certified by peer review) is the author/funder, who has granted bioRxiv a license to display the preprint in perpetuity. It is made available under aCC-BY-NC 4.0 International license.

Abstract

Background In addition to the processes structuring free-living communities, host-associated microbial communities (i.e., microbiotas) are directly or indirectly shaped by the host. Therefore, microbiota data have a hierarchical structure where samples are nested under one or several variables representing host-specific features. In addition, microbiota data are often collected across multiple levels of biological organization. Current statistical methods do not accommodate this hierarchical data structure, and therefore cannot explicitly account for the effects of host-specific features on structuring the microbiota.

Methods We introduce a unifying model-based framework developed specifically for analyzing host-microbiota data spanning multiple levels of biological organization. While we chose to discern among the effects of host species identity, host phylogeny, and host traits in structuring the microbiota, the presented framework can straightforwardly accommodate any recorded data that includes host-specific features. Other key components of our modeling framework are the powerful yet familiar outputs: (i) model-based ordination to visualize the main patterns in the data, (ii) co-occurrence networks to visualize microbe-to-microbe associations, and (iii) variance partitioning to asses the explanatory power of the included host-specific features and how influential these are in structuring the microbiota.

Results The developed framework was applied to published data on marine sponge-microbiota. We found that a series of host traits that are likely phylogenetically conserved underpinned differences in both abundance and species richness among sites. When controlling for these differences, microbiota composition among sites was confounded by numerous site and host-specific features. At the host level, host traits always emerged as the prominent host-specific feature structuring the microbiota.

Conclusions The proposed framework can readily be applied to a wide range of microbiota systems spanning multiple levels of biological organization, allowing researchers to systematically tease apart the relative importance of recorded and/or measured host-specific features in structuring microbiota. The study of free-living species communities have significantly benefited from the increase in model-based approaches. We believe that it is time for research on host-microbiota to leverage the strengths of a unifying model-based framework.

bioRxiv preprint doi: https://doi.org/10.1101/137943; this version posted May 14, 2017. The copyright holder for this preprint (which was not certified by peer review) is the author/funder, who has granted bioRxiv a license to display the preprint in perpetuity. It is made available under aCC-BY-NC 4.0 International license.

Introduction

Ecological communities are the product of both stochastic and deterministic processes. While environmental factors may set the upper bound on carrying capacity, competitive and facilitative interactions within and among taxa determine the identity of the species present in local communities. Ecologists are often interested in inferring ecological processes from patterns and determining their relative importance for the community under study ([39]). During the last few years, there has been a growing interest in developing new statistical methods aimed toward ecologists and the analysis of multivariate community data (see e.g., [17] and references within). There are many metrics for analyzing such data, however, these have a number of drawbacks, including uncertainty of selecting the most appropriate null models/randomization tests, low statistical power, and the lack of possibilities for making predictions. One framework which has become increasingly popular in ecology is joint species distribution models (JSDMs,[28, 40, 25]). JSDMs are an extension of generalized linear mixed models (GLMMs, [3]) where multiple species are analyzed simultaneously, with or without measured environmental data, revealing community-level responses to environmental change. Because JSDMs are an extension of GLMMs, they can partition variance among fixed and random effects to assess the relative contribution of different ecological processes, such as habitat filtering, biotic interactions and environmental variability ([25]). Also, with the increase of trait-based and phylogenetic data in community ecology, together with the growing appreciation that species interactions are constrained by the "phylogenetic baggage" they inherit from their ancestors ([34]), this type of models can further accommodate information on both species traits and phylogenetic relatedness among species ([14, 15, 1, 25]). As such, JSDMs represents a rigorous statistical framework which allows ecologists to gain a more mechanistic view of the processes structuring ecological communities ([40]).

In parallel to recent developments in community ecology, there is the growing field of microbial ecology studying both free-living and host-associated communities (i.e., microbiotas). While microbial ecologists can adapt many of the new statistical approaches developed for traditional multivariate abundance data (see e.g., [4]), researchers studying microbiotas need to consider an additional layer of processes structuring the focal community: microbiotas are also shaped directly or indirectly by their hosts. Interactions between hosts and microbes often involve long-lasting and sometimes extremely intimate relationships where the host animal may have evolved a capacity to directly control the identity and/or abundance of its microbial symbionts ([21]). Similarly to an environmental niche, host-specific features can be viewed as a multidimensional composite of all the host-specific factors governing microbial abundances and/or occurrences within a host. These may represent everything from broad evolutionary relationships among host species ([11]) to distinct ecological processes, such as the production of specific biomolecules within a single host species

bioRxiv preprint doi: https://doi.org/10.1101/137943; this version posted May 14, 2017. The copyright holder for this preprint (which was not certified by peer review) is the author/funder, who has granted bioRxiv a license to display the preprint in perpetuity. It is made available under aCC-BY-NC 4.0 International license.

([18]). Furthermore, microbiotas often encompass multiple levels of biological organization, as e.g., samples may be collected from different body sites on numerous host individuals, and/or from different host species across larger spatial scales. At each level of biological organization, a different set of processes are likely to be influencing the microbiota.

While a few recent JSDMs have been applied to microbiota data ([1, 5, 36, 44]), none of these models explicitly and transparently account for the aforementioned host-specific features. This extra layer of processes creates a hierarchical data structure where samples are nested under one or several nominal variables representing recorded and/or measured host-specific features. On the other hand, as JSDMs are naturally multi-levelled, they can easily account for such a hierarchical data structure, including the hierarchy implicit in data spanning multiple levels of biological organization ([24, 20]). An example of such a data set is the gut microbiota of the Amboselli baboons (see e.g., [37]), where individual baboons are raised in matriarchal family groups which are part of larger social groups. Individuals may disperse from their family groups to other social groups when reaching adulthood. Individual baboons are therefore nested within both family and social groups, and researchers may want to investigate what processes acting on which social level of organization are most likely governed the gut microbiota.

Discerning among processes through joint distribution models

How processes related to host-specific features structure the microbiota are largely unknown. At the same time, to analyze such data requires a unifying, model-based framework capable of discerning amongst various host-specific features spanning multiple levels of biological organization. To fill this gap, we propose a novel JSDM framework specifically aimed at analyzing microbiota data which explicitly accounts for host-specific features across multiple levels of biological organization. Other key components of our proposed modeling framework include: (i) model-based ordination to visualize the main patterns in the data (ii) co-occurrence networks to visualize microbe-to-microbe associations, and (iii) variance partitioning to asses the explanatory power of the included host-specific features and their influence in structuring the microbiota (Figure 2). While our models can discern among the effects of host species identity, host phylogeny and host traits, they can straightforwardly accommodate any recorded and/or measured data on host-specific features. However, information on host phylogenetic relatedness and host traits are particularly useful in order to disentangle whether the microbiota under study is non-randomly structured among the branches of a host phylogeny such that related host species harbor more similar microbes (i.e., indicating vertical transmission) or whether the microbiota is non-randomly structured among environments reflecting different host traits (i.e., indicating horizontal transmission).

bioRxiv preprint doi: https://doi.org/10.1101/137943; this version posted May 14, 2017. The copyright holder for this preprint (which was not certified by peer review) is the author/funder, who has granted bioRxiv a license to display the preprint in perpetuity. It is made available under aCC-BY-NC 4.0 International license.

By applying our developed modeling framework to sponge-microbiota data, we set out to investigate a set of fundamental, but non-mutually exclusive questions of interest. Broadly, we are interested in whether the sponge microbiota are governed by processes at the site and/or host species level. More specifically we ask whether the microbiota associated with: (i) the same host species and/or (ii) phylogenetically closely related host species and/or (iii) host species with similar traits, are more similar irrespective of the spatial distance between the sites where they were collected. We also investigate whether host species in closely located areas harbor more similar microbiotas than host species collected in sites farther apart. Finally, we generate microbe-to-microbe association networks using our proposed framework, but acknowledge that we do not have any *a-priori* hypotheses regarding which microbes are more or less likely to be co-occur. To our knowledge, this is the first unifying model-based framework specifically developed for analyzing host-microbiota.

Materials and methods

Sponge microbiota as a case study

To illustrate our modeling framework, we acquired data on marine sponge-microbiota from different host species collected at different geographic sites across the globe (Figure 1, Table S1). As marine sponges are commonly divided into two groups reflecting a suit of morphological and physiological traits– coined *High* and *Low Microbial Abundance* (HMA/LMA) sponges–collection sites are nested within host species which are further nested within one of the two traits. While the HMA-LMA division in a strict sense refers to the abundance of microbes harbored by the host, HMA sponges have a denser interior, including narrower aquiferous canals and smaller choanocytes compared to LMA sponges whose architecture are more fitted for pumping large volumes of water ([38]). As a consequence, HMA and LMA sponges tend to harbor different microbiotas, with the latter often showing a higher similarity to the free-living microbial community present in the surrounding sea water ([2, 33]).

Data compilation

To assess variation in microbial abundances and co-occurrences across different sponges species collected at different sites, we compiled a data set of sponge-associated bacterial 16S rRNA gene clone-library sequences published in NCBI GenBank (http://www.ncbi.nlm.nih.gov) between September 2007 and August 2014. All sponge species in the data set were required to be present in at least two different collection sites and be associated with at least 10

bioRxiv preprint doi: https://doi.org/10.1101/137943; this version posted May 14, 2017. The copyright holder for this preprint (which was not certified by peer review) is the author/funder, who has granted bioRxiv a license to display the preprint in perpetuity. It is made available under aCC-BY-NC 4.0 International license.

different sequences per site. The final data set contained a total of 3874 nearly full-length 16S rRNA gene sequences from 9 HMA and 10 LMA sponge species collected at 48 different sites (n_{HMA}=28, n_{LMA}=20) across the Atlantic, Pacific Ocean, Mediterranean and Red Seas (Figure 1, Table S1). The 16S rRNA gene sequences were aligned and clustered into operational taxonomic units (OTUs) representing family-level (at 90% nucleotide similarity, [42, 32]) using mothur v.1.32.1 ([31]). At higher and lower sequence similarities, OTU clusters tended to become either too narrow or too broad, generating too sparse data for our models. Finally, as clone-libraries do not circumvent the need for cultivation, the OTUs modelled here correspond to the most common members of the sponge-microbiota.

Phylogenetic reconstructions

We retrieved nearly full-length sponge 18S rRNA gene sequences published in NCBI GenBank (http://www.ncbi.nlm.nih.gov) (see e.g., [10]). Sequences were aligned using the default options in ClustalW (1.83) ([16]). The phylogenetic relationship between the sponge species were reconstructed by implementing a HKY + Γ_4 substitution model using BEAST (1.7.4) ([6]). For a few host species (*I. oros, H. simulans, M. methanophila and X. testudinaria*), the 18S rRNA gene sequence was unavailable. In these cases, we constrained the sponge species to the clade containing its genera.

A posterior distribution of phylogenies were sampled using Markov Chain Monte Carlo (MCMC) simulations as implemented in BEAST. We ran 4 independent chains each for 20 million generations saving every 4000th sample and discarding the first 25% as burn-in. This resulted in 20,000 generations from the posterior distribution. Convergence was evaluated using Tracer (v1.5) ([30]). We summarized the output of the four chains as a consensus phylogeny. Assumeing Brownian motion so that each covariance between host species i and host species j is proportional to their shared branch length from the most recent common ancestor ([7]), we used the variance-covariance matrix of the consensus phylogeny $\Sigma(\text{phylo})$ as prior information in Equation 3, such that $\boldsymbol{\mu}(\text{phylo})_s \sim \mathcal{MVN}(\mathbf{0}, \Sigma(\text{phylo}))$. Note that as the host species-specific variance i.e., the diagonal elements of the variance-covariance matrix is scaled to one by the construction of $\Sigma(\text{phylo})$, we multiplied it with a scaling factor τ as seen in the formulation in (3).

Joint species distribution models

We developed a Bayesian joint species distribution modeling framework to jointly model the abundance and co-occurrence of OTUs across multiple sites, while also accounting for host species identity, host phylogenetic relatedness, and host traits (HMA and LMA, hereafter termed *ecotype*). Another important feature of the models we propose is the inclusion of latent factors, serving three main purposes. First, they allow for a parsimonious yet flexible way

bioRxiv preprint doi: https://doi.org/10.1101/137943; this version posted May 14, 2017. The copyright holder for this preprint (which was not certified by peer review) is the author/funder, who has granted bioRxiv a license to display the preprint in perpetuity. It is made available under aCC-BY-NC 4.0 International license.

of modeling correlations between a large number of taxa. That is, given the number of taxa recorded often has the same order or exceeds the number of sites, as is characteristic of most multivariate abundance data including the one analyzed here, modeling the covariation between all taxa using an unstructured correlation matrix is often unreliable due to the large number of elements in the matrix that need to be estimated ([40]). Using latent factors instead offers a more practical solution, via rank reduction, to model correlations in such high dimensional settings. Second, latent factors allow for performing model-based unconstrained and residual ordination in order to visualize the main patterns in the data ([12, 13]). While traditional distance-based ordination techniques easily confound location and dispersion effects ([41]), model-based ordination properly models the mean-variance relationship, and can therefore accurately detect differences between the two. Third, latent factors allow for inferring associative networks identified by correlations and partial correlations ([24]).

We considered two response types commonly encountered in ecology and biogeography; negative binomial regression for overdispersed counts and probit regression for presence-absence. As such, the response matrix being modelled consisted of either counts or presence-absence of n OTUs observed at m sites. The rows of the response matrix have a hierarchical structure typical for many microbiota data. Specifically, the $m = 48$ sites are nested within the $s = 19$ host species, with the 19 host species nested within one of $r = 2$ ecotypes (Figure 2). Due to their lack of information, OTUs with less than 5 presences across sites and with a total abundance of less than 5 were removed, resulting in 65 modelled OTUs.

NB model: Due to the presence of overdispersion in the counts, a negative binomial distribution with a quadratic mean-variance relationship was assumed for the response matrix y_{ij}, such that $\mathrm{Var}(y_{ij}) = \upsilon_{ij} + \phi_j \upsilon_{ij}^2$ where ϕ_j is the OTU-specific overdispersion parameter. The mean abundance was related to the covariates using a log link function. We denote the response and mean abundance of OTU j at site i by y_{ij} and υ_{ij}, respectively.

Probit model: Presence ($y_{ij} = 1$) or absence ($y_{ij} = 0$) of OTU j at site i was modelled by a probit regression, implemented as $y_{ij} = 1_{z_{ij}>0}$ where the latent liability z_{ij} is a linear function of the covariates, including the probit link function. Below, we present specifications for the negative binomial (NB) model only, as the probit model description is similar except the distribution assumed at the response level of the model (S1).

Let $\mathcal{N}(\mu, \sigma^2)$ denote a normal distribution with mean μ and variance σ^2, and analogously, let $\mathcal{MVN}(\boldsymbol{\mu}, \Sigma)$ denote a multivariate normal distribution with mean vector and covariance matrix Σ. Then, we have the model formulation

bioRxiv preprint doi: https://doi.org/10.1101/137943; this version posted May 14, 2017. The copyright holder for this preprint (which was not certified by peer review) is the author/funder, who has granted bioRxiv a license to display the preprint in perpetuity. It is made available under aCC-BY-NC 4.0 International license.

as follows

$$y_{ij} \sim \text{Negative-Binomial}(\upsilon_{ij}, \phi_j); \quad i = 1, \ldots, 48; \quad j = 1, \ldots, 65 \tag{1}$$

$$\log(\upsilon_{ij}|\boldsymbol{z}_i) = \alpha_i + \beta_j + \sum_{q=1}^{2} Z_{iq}^{S} \lambda_{qj}^{S} + \sum_{q=1}^{2} Z_{s[i]q}^{H} \lambda_{qj}^{H}; \quad q = 1, \ldots, 2 \tag{2}$$

$$\begin{aligned}
\beta_j &\sim Cauchy(0, 2.5) \\
\alpha_i &\sim \mathcal{N}(\mu_i, \sigma^2(\text{host})) \\
\mu_i &= \mu(\text{host})_{s[r]} + \tau * \mu(\text{phylo})_s; \quad r = 1, 2;\ s = 1, \ldots, 19 \\
\mu(\text{host})_{s[r]} &\sim \mathcal{N}(\mu(\text{ecotype})_r, \sigma^2(\text{ecotype})) \\
\mu(\text{ecotype})_r &\sim Cauchy(0, 2.5) \\
\boldsymbol{\mu}(\text{phylo})_s &\sim \mathcal{MVN}(\mathbf{0}, \Sigma(\text{phylo}))
\end{aligned} \tag{3}$$

To clarify the above formulation, the subscript r indexes ecotype, s indexes host species and i indexes sites, such that "$s[i]$" and "$s[r]$" means "site i nested within host species s" and "host species s nested within ecotype r", respectively. In Equation (2), the quantities α_i and β_j represent site and OTU-specific effects, respectively. The former adjusts for differences in site total abundance (species richness in the probit case), whereas the latter controls for differences in OTU total abundance (OTU prevalence across sites in the probit case). From a purely statistical point of view, this can be thought of as a model-based analog of studying alpha and beta diversity, respectively. The inclusion of α_i serves two main purposes. First and foremost, including α_i allows us to account for the hierarchical structure of the data and its effect on site total abundance (species richness in the probit case) specifically. In particular, to account for site i being nested within host species s which in turn is nested within ecotype r, the site effects α_i's are drawn from a normal distribution with a mean that is a linear function of both a host-specific mean $\mu(\text{host})_{s[r]}$ and a host-specific phylogenetic effect $\boldsymbol{\mu}(\text{phylo})_s$ (Equation 3). Furthermore, the host effects themselves are drawn from a normal distribution with a ecotype-specific mean $\mu(\text{ecotype})_r$. Second, it means the resulting ordinations constructed by the latent factors at the site Z_{iq}^{S} and host species $Z_{s[i]q}^{H}$ level are in terms of composition only, as opposed to a composite of site total abundance (species richness in the probit case) and composition (i.e. microbiota structure) when site effects are not included ([12]). In other words, by accounting for the hierarchical structure present in the data, the model-based ordinations are able to distinguish between microbiota composition and structure. It also means that the corresponding factor loadings λ_{qj}^{S} and λ_{qj}^{H} which quantify each OTU's response to the latent factors and subsequently

bioRxiv preprint doi: https://doi.org/10.1101/137943; this version posted May 14, 2017. The copyright holder for this preprint (which was not certified by peer review) is the author/funder, who has granted bioRxiv a license to display the preprint in perpetuity. It is made available under aCC-BY-NC 4.0 International license.

the correlations among OTUs at the two different levels of biological organization are driven by OTU-specific effects only, as opposed to correlations additionally induced by site and host-specific features.

Note that, in contrast to the means μ's, the variance parameters σ^2(host) and σ^2(ecotype) are common across all hosts and ecotypes. This implies that, *a-priori*, hosts and ecotypes can differentiate in location (mean) but not in dispersion (variance). However, as we will see later in the Results section, the ordinations for hosts and ecotypes can still, *a-posteriori*, vary substantially in terms of location and dispersion. We fitted each model with and without site effects α_i included, so that two types of ordinations and association networks were constructed. When site effects were included, the ordinations on both levels of biological organization are in terms of microbiota composition, whereas when site effects are not included, the ordinations represent microbiota structure. The inclusion of α_i also allows us to discern among OTU-to-OTU correlations induced by OTU-specific effects from those induced by site and host-specific features. For the model without site effects α_i included, its associated nested structure were removed from Equation (2), such that $\log(\upsilon_{ij}|\boldsymbol{z}_i) = \beta_j + \sum_{q=1}^{2} Z_{iq}^{S}\lambda_{qj}^{S} + \sum_{q=1}^{2} Z_{s[i]q}^{H}\lambda_{qj}^{H}$. As is conventional with ordination, we set $q = 2$ so that once fitted, the latent factors $Z_{i,q} = (Z_{i1}, Z_{i2})$ were plotted on a scatter plot to visualize the main patterns in the data ([12]). From the corresponding factor loadings λ_{qj}, a variance-covariance matrix was computed as $\Omega = \lambda_{1j}(\lambda_{2j})^T$, and subsequently converted to a correlation matrix and plotted as a OTU-to-OTU association network ([24]).

To complete the above formulation, we assigned priors to the appropriate hyperparameters. For the OTU-specific overdispersion parameters ϕ_j (Equation 1), we chose to assign a weakly-informative Gamma prior, Gamma$(0.1, 0.1)$. The standard deviations for host σ(host) and ecotype σ(ecotype) in Equations (2)-(3) were assigned uniform priors Unif$(0, 30)$. The latent factors in Equation (2) on the site Z_{iq}^{S} and host species Z_{iq}^{H} level were assigned normal priors $\mathcal{N}(0, 1)$. The corresponding OTU-specific coefficients, i.e., the λ_{qj}^{S}'s and the λ_{qj}^{H}'s in Equation (2) were assigned Cauchy priors with center and scale parameters of 0 and 2.5, respectively, while taking to account the appropriate constraints for parameter identifiability (see citeHui2015, for details). The Cauchy distribution was used because it is good example of a weakly-informative normal prior ([9]). Finally, the phylogenetic scale parameter τ was drawn from a weakly-informative exponential prior with a rate parameter of 0.1.

Variance partitioning

One of the main advantages of the differing levels in the hierarchy in Equations (1)-(3) is that we can calculate the total variance of the μ_i's and partition this variance into components reflecting variation in site total abundance (species richness in the probit case) attributable to differences in host species identity $\mu(\text{host})_s$, host phylogenetic relatedness $\mu(\text{phylo})_s$ and host traits $\mu(\text{ecotype})_r$. This means that we can asses the explanatory power of the host-specific features

bioRxiv preprint doi: https://doi.org/10.1101/137943; this version posted May 14, 2017. The copyright holder for this preprint (which was not certified by peer review) is the author/funder, who has granted bioRxiv a license to display the preprint in perpetuity. It is made available under aCC-BY-NC 4.0 International license.

and how influential each of them are in structuring the microbiota. Such a variance decomposition is analogous to sum-of-squares and variance decompositions seen in Analysis of Variance (ANOVA) and linear mixed models ([23]).

Let V_{total} denote the total variance of the μ_i's, while V_{host}, V_{phylo} and V_{ecotype} denote the variances due to host species identity, host phylogeny and host ecotype, respectively. Then we have,

$$V_{\text{total}} = V_{\text{host}} + V_{\text{phylo}} + V_{\text{ecotype}} + (\mu(\text{ecotype})_{LMA} - \mu(\text{ecotype})_{HMA})^2, \quad \text{where} \tag{4}$$

$$V_{\text{ecotype}} = \sigma^2(\text{ecotype}) \tag{5}$$

$$V_{\text{host}} = \sigma^2(\text{host}) \tag{6}$$

$$V_{\text{phylo}} = \tau^2 \tag{7}$$

Where $\sigma^2(\text{host})$ reflects the intraspecific variation among sites nested within host species with small values of $V_{\text{host}}/V_{\text{total}}$ implying that sites nested within the same host species are more similar within than between host species. τ^2 corresponds the intraspecific variation among sites nested within host species that can be attributed to hosts' phylogenetic relatedness, meaning that small values of $V_{\text{phylo}}/V_{\text{total}}$ provide evidence that the host phylogeny has little influence on variation in site total abundance (species richness in probit case). $\sigma^2(\text{ecotype})$ accounts for intraspecific variation among host species nested within the two ecotypes, whereas $(\mu(\text{ecotype})_{LMA} - \mu(\text{ecotype})_{HMA})^2$ is the difference in variation between the two ecotypes. Therefore, $(\mu(\text{ecotype})_{LMA} - \mu(\text{ecotype})_{HMA})^2/V_{\text{total}}$ represents the proportion of total variation in site total abundance (species richness in the probit case) driven by ecotype. That is, if the proportion $V_{\text{ecotype}}/V_{\text{total}}$ is small compared to $(\mu(\text{ecotype})_{LMA} - \mu(\text{ecotype})_{HMA})^2/V_{\text{total}}$, then host species' microbiota are more similar within rather than between ecotypes.

We used Markov Chain Monte Carlo (MCMC) simulation method by running JAGS ([26]) in R ([29]) through the *rjags* ([19]) package to sample from the joint posterior distribution of the model parameters. We ran 1 chain with dispersed initial values for 100,000 iterations saving every $10^t h$ sample and discarding the first 50% of samples as burn-in. We evaluated convergence of model parameters by visually inspecting trace and density plots using the R packages *coda* ([27]) and *mcmcplots* ([22]).

Results

We did not observe any large qualitative differences between the negative binomial (NB) and probit models of our framework. As noted above, an interesting difference between the two models is the interpretation of the row and

bioRxiv preprint doi: https://doi.org/10.1101/137943; this version posted May 14, 2017. The copyright holder for this preprint (which was not certified by peer review) is the author/funder, who has granted bioRxiv a license to display the preprint in perpetuity. It is made available under aCC-BY-NC 4.0 International license.

column totals. Modeling counts means that row and column totals correspond to site and OTU total abundance, respectively, rather than species richness and OTU prevalence across sites as in the case of presence-absences. Even if the two are very similar, the latter has a more straightforward interpretation as alpha and beta diversity. We present the main results for both models below, but relegate figures associated to the probit model to the supplementary material.

At the site level, without adjusting for differences among sites (i.e. not including α_i), host ecotype appeared as the major host-specific feature driving differences in microbiota structure (Figure 3A-B, S2A-B). After adjusting for site effects, while simultaneously accounting for host species identity, host phylogenetic relatedness and host ecotype, sites clustered, i.e., they harbored similar microbiota composition, to a lesser extent by host ecotype (Figure 3C-D, S2C-D). The variance partitioning showed that differences among sites in terms of abundance and richness were largely driven by host phylogenetic relatedness (Figure 4, S3), suggesting that ecotype is phylogenetically conserved within *Porifera*. It also indicates that composition among sites, similarly to abundance and richness, is confounded by site and host-specific features, such as geographic distance, host species identity, host phylogenetic relatedness and host ecotype. For example, a few sites clustered by host species (e.g., HMA hosts *Aplysina cualiformis*, *Aplysina fluva*, *Ircinia felix*, and *Ircinia oros*), but at closer inspection, the geographic distance between several of these sites were low (Figure 3C, Figure S2C). At the host-species level, hosts always clustered according to ecotype, indicating that the set of traits encompassing HMA and LMA hosts are indeed important for structuring the microbiota (Figure 5A-B, S4A-B).

A closer look at α_i, the parameter adjusting for site effects, showed that sites belonging to the same host species and sites belonging to either of the two host ecotypes often had similar posterior means, with HMA hosts typically having narrower credible intervals (Figure 6A, S5A). However, these differences were not present in the mean parameter of α_i, i.e., the $\mu(\text{host})_{s[r]}$ (Figure 6B, S5B), further indicating that microbiota composition, more than differences in abundance and richness, is driving the observed HMA-LMA dichotomy.

We did not find any distance-decay relationship where microbiota similarity among sites decrease with increasing geographic distance. However weak, we observed that HMA and LMA hosts had opposite slopes in the model not controlling for site effects, indicating that LMA microbiota may be more influenced by local environmental conditions (Figures S1,S6). Interestingly, for the NB model, the slope of LMA hosts switched sign in the model adjusted for site effects. (Figure S1).

We generated OTU-to-OTU association networks where links between OTUs represented either positive and negative abundance correlations and co-occurrences with at least 95% posterior probability. On one hand, by not adjusting for site effects, correlations between OTUs are induced by not only OTU-specific effects, but also by site and host-

bioRxiv preprint doi: https://doi.org/10.1101/137943; this version posted May 14, 2017. The copyright holder for this preprint (which was not certified by peer review) is the author/funder, who has granted bioRxiv a license to display the preprint in perpetuity. It is made available under aCC-BY-NC 4.0 International license.

specific features. We found many more correlations in the model not controlling for site effects (Figures 7A-B, S7A-B) compared to the model that did (Figure 7C-D, S7C-D). The site level (Figures 7A-C, S7A-C) generally had more correlations compared to the host species level (Figure 7B-D, S7B-D). On the site level, correlations were likely induced by, in addition to host-specific features, site effects such as geographic distance, coexisting host species and/or similar environmental preferences among OTUs, whereas on the host species level, correlations were only induced by host-specific features. The probit model detected more correlations on both levels compared to the NB model (S7). This is likely due to the difference in the nature of the correlations, i.e., co-occurrences (probit model) versus abundance correlations (NB model).

Discussion

Discerning amongst the many processes structuring microbiotas is one of the big new challenges facing ecology and evolution. However, the complexity of these communities often preclude their understanding, and we currently lack a mechanistic view of the processes structuring these systems. Motivated by these challenges, we developed a joint species distribution modeling (JSDM) framework to enhance our understanding of how host-specific features influence and structure the microbiota, both in terms of the abundance/species richness and composition of microbes. The presented framework builds upon and extends existing JSDMs by specifically targeting the hierarchical structure typically characterizing microbiota data. For example, our framework can be seen as microbiota adapted phylogenetic generalized linear mixed models where we model host species traits and phylogenetic relatedness on the rows of the response matrix, as opposed to on the columns as seen in the typical specification of these models ([14]).

Whether host phylogeny and/or host traits structure the microbiota reveal important information about the underlying processes. We found a strong phylogenetic signal on microbial abundance and species richness among hosts, but at the same time, we did not observe a clear clustering by host phylogeny. Instead, the sponge-microbiota always showed a strong clustering by host traits (i.e. HMA/LMA), indicating (1) that host traits may be phylogenetically conserved within *Porifera* and/or (2) that the microbiota may be adapted to the different host environments associated with the two traits. Traditional ordination methods, such as principal coordinate analysis (PCoA) and non-metric multidimensional scaling (NMDS) does not allow for such a systematic dissection of the patterns and the likely processes structuring host-microbiotas.

Other advantages compared to traditional ordination methods are that model-based ordination is implemented and developed by directly accommodating the statistical properties of the data at hand ([12]). Failure to account for, e.g.,

bioRxiv preprint doi: https://doi.org/10.1101/137943; this version posted May 14, 2017. The copyright holder for this preprint (which was not certified by peer review) is the author/funder, who has granted bioRxiv a license to display the preprint in perpetuity. It is made available under aCC-BY-NC 4.0 International license.

the mean–variance relationship can lead to misleading results (see [41] for details and discussion). Another advantage of our modeling framework is that the constructed ordinations are able to distinguish between microbiota composition and structure. For instance, we found that on the host species level, ecotype (HMA/LMA) emerged as the major host-specific feature driving microbiota structure and composition, whereas on the site level, structure and composition was confounded by numerous factors. Furthermore, calculating total variance and partitioning this into components reflecting variation attributable to different host-specific features, such as host traits and phylogenetic relatedness, allows researchers to assess the relative importance of possible ecological processes.

It has become increasingly popular in microbial ecology to visualize OTU-to-OTU association networks from correlations (e.g. [8, 43]). A key feature of the presented framework is the use of latent factors as a parsimonious approach for modeling correlations between a large number of taxa. Beyond OTU-specific effects, such as e.g., interspecific interactions, correlations amongst OTUs may be induced by site and/or host-specific features. Therefore, by modeling the microbiota on multiple levels of biological organization, while simultaneously controlling for site effects and its hierarchical structure (i.e. the host-specific features), it is possible to gain a better understanding of the possible interaction structures. However, as these associations are of correlative nature, they should not be regarded as ecological interactions, but merely as hypotheses of such ([24, 35]).

Finally, the presented framework can readily be applied to a wide range of microbiota systems spanning multiple levels of biological organization, where the main interest lies in teasing apart the relative importance among host-specific features in structuring the microbiota. It can further be adapted to accommodate additional information, such as e.g., phylogenetic relatedness among microbes, spatial distance between sites, and/or environmental covariates directly acting on the hosts. Such a flexible modeling framework offers many exciting avenues for methodological advancements that will help to enhance our understanding of the numerous processes structuring host-microbiotas.

References

[1] Tuomas Aivelo and Anna Norberg. Parasite-microbiota interactions potentially affect intestinal communities in wild mammals. *bioRxiv*, 2016.

[2] Johannes R. Björk, C. Díez-Vives, Rafel Coma, Marta Ribes, and José M. Montoya. Specificity and temporal dynamics of complex bacteria-sponge symbiotic interactions. *Ecology*, 94(12):2781–2791, 2013.

bioRxiv preprint doi: https://doi.org/10.1101/137943; this version posted May 14, 2017. The copyright holder for this preprint (which was not certified by peer review) is the author/funder, who has granted bioRxiv a license to display the preprint in perpetuity. It is made available under aCC-BY-NC 4.0 International license.

[3] Benjamin M. Bolker, Mollie E. Brooks, Connie J. Clark, Shane W. Geange, John R. Poulsen, M. Henry H. Stevens, and Jada-Simone S. White. Generalized linear mixed models: a practical guide for ecology and evolution. *Trends in Ecology & Evolution*, 24(3):127–135, 2009.

[4] Miklós Bálint, Mohammad Bahram, A. Murat Eren, Karoline Faust, Jed A. Fuhrman, Björn Lindahl, Robert B. O'Hara, Maarja Öpik, Mitchell L. Sogin, Martin Unterseher, and Leho Tedersoo. Millions of reads, thousands of taxa: microbial community structure and associations analyzed via marker genes. *FEMS Microbiology Reviews*, 40(5):686, 2016.

[5] James S. Clark, Diana Nemergut, Bijan Seyednasrollah, Phillip J. Turner, and Stacy Zhang. Generalized joint attribute modeling for biodiversity analysis: median-zero, multivariate, multifarious data. *Ecological Monographs*, 87(1):34–56, 2017.

[6] A.J. Drummond, M.A. Suchard, D. Xie, and Rambaut A. Bayesian phylogenetics with BEAUti and the BEAST 1.7. *Molecular Biology And Evolution*, 12:1969–1973, 2012.

[7] Joseph Felsenstein. Phylogenies and the Comparative Method. *The American Naturalist*, 125(1):1–15, 1985.

[8] Jonathan Friedman and Eric J. Alm. Inferring Correlation Networks from Genomic Survey Data. *PLOS Computational Biology*, 8(9):1–11, 09 2012.

[9] Andrew Gelman, Aleks Jakulin, Maria Grazia Pittau, and Yu-Sung Su. A Weakly Informative Default Prior Distribution for Logistic and Other Regression Models. 2(4):1360–1383, 2008.

[10] Volker Gloeckner, Markus Wehrl, Lucas Moitinho-Silva, Christine Gernert, Peter Schupp, Joseph R. Pawlik, Niels L. Lindquist, Dirk Erpenbeck, Gert Wörheide, and Ute Hentschel. The HMA-LMA Dichotomy Revisited: an Electron Microscopical Survey of 56 Sponge Species. *The Biological bulletin*, 227(1):78–88, 2014.

[11] Mathieu Groussin, Florent Mazel, Jon G. Sanders, Chris S. Smillie, Sébastien Lavergne, Wilfried Thuiller, and Eric J. Alm. Unraveling the processes shaping mammalian gut microbiomes over evolutionary time. *Nature Communications*, 8:14319EP, Feb 2017.

[12] Francis K C Hui, Sara Taskinen, Shirley Pledger, Scott D. Foster, and David I. Warton. Model-based approaches to unconstrained ordination. *Methods in Ecology and Evolution*, 6(4):399–411, 2015.

[13] Francis K.C. Hui. boral–Bayesian Ordination and Regression Analysis of Multivariate Abundance Data in R. *Methods in Ecology and Evolution*, 2016.

bioRxiv preprint doi: https://doi.org/10.1101/137943; this version posted May 14, 2017. The copyright holder for this preprint (which was not certified by peer review) is the author/funder, who has granted bioRxiv a license to display the preprint in perpetuity. It is made available under aCC-BY-NC 4.0 International license.

[14] Anthony R. Ives and Matthew R. Helmus. Phylogenetic metrics of community similarity. *The American naturalist*, 176(5):E128–E142, 2010.

[15] Arne Kaldhusdal, Roland Brandl, Jörg Müller, Lisa Möst, and Torsten Hothorn. Spatio-phylogenetic multispecies distribution models. *Methods in Ecology and Evolution*, 6(2):187–197, 2015.

[16] M.A. Larkin, G. Blackshields, N.P. Brown, R. Chenna, P.A. McGettigan, H. McWilliam, F. Valentin, I.M. Wallace, A. Wilm, R. Lopez, J.D. Thompson, T.J. Gibson, and D.G. Higgins. Clustal W and Clustal X version 2.0. *Bioinformatics*, 23(21):2947, 2007.

[17] Pierre Legendre and Olivier Gauthier. Statistical methods for temporal and space-time analysis of community composition data. *Proceedings of the Royal Society of London B: Biological Sciences*, 281(1778), 2014.

[18] Shirong Liu, Andre Pires da Cunha, Rafael M. Rezende, Ron Cialic, Zhiyun Wei, Lynn Bry, Laurie E. Comstock, Roopali Gandhi, and Howard L. Weiner. The Host Shapes the Gut Microbiota via Fecal MicroRNA. *Cell Host & Microbe*, 19(1):32–43, 2016.

[19] Plummer Martyn, Alexey Stukalov, and Matt Denwood. Bayesian Graphical Models using MCMC. *R News*, 6(1):7–11, 2006.

[20] Joseph B. Maxwell, William E. Stutz, and Pieter T. J. Johnson. Multilevel Models for the Distribution of Hosts and Symbionts. *PLOS ONE*, 11(11):1–15, 11 2016.

[21] Margaret McFall-Ngai, Michael G. Hadfield, Thomas C.G. Bosch, Hannah V. Carey, Tomislav Domazet-Lošo, Angela E. Douglas, Nicole Dubilier, Gerard Eberl, Tadashi Fukami, Scott F. Gilbert, Ute Hentschel, Nicole King, Staffan Kjelleberg, Andrew H. Knoll, Natacha Kremer, Sarkis K Mazmanian, Jessica L. Metcalf, Kenneth Nealson, Naomi E Pierce, John F. Rawls, Ann Reid, Edward G. Ruby, Mary Rumpho, Jon G. Sanders, Diethard Tautz, and Jennifer J. Wernegreen. Animals in a bacterial world, a new imperative for the life sciences. *Proceedings of the National Academy of Sciences*, 110(9):3229–3236, 2013.

[22] Curtis S. McKay. Create Plots from MCMC Output. *R News*, 2015.

[23] Shinichi Nakagawa and Holger Schielzeth. A general and simple method for obtaining R2 from generalized linear mixed-effects models. *Methods in Ecology and Evolution*, 4(2):133–142, 2013.

bioRxiv preprint doi: https://doi.org/10.1101/137943; this version posted May 14, 2017. The copyright holder for this preprint (which was not certified by peer review) is the author/funder, who has granted bioRxiv a license to display the preprint in perpetuity. It is made available under aCC-BY-NC 4.0 International license.

[24] Otso Ovaskainen, Nerea Abrego, Panu Halme, and David Dunson. Using latent variable models to identify large networks of species-to-species associations at different spatial scales. *Methods in Ecology and Evolution*, 7(5):549–555, 2016.

[25] Otso Ovaskainen, Gleb Tikhonov, Anna Norberg, F. Guillaume Blanchet, Leo Duan, David Dunson, Tomas Roslin, and Nerea Abrego. How to make more out of community data? A conceptual framework and its implementation as models and software. *Ecology Letters*, 2017.

[26] Martyn Plummer. *JAGS: A program for analysis of Bayesian graphical models using Gibbs sampling*, 2003.

[27] Martyn Plummer, Nicky Best, Kate Cowles, and Karen Vines. CODA: Convergence Diagnosis and Output Analysis for MCMC. *R News*, 6(1):7–11, 2006.

[28] Laura J. Pollock, Reid Tingley, William K. Morris, Nick Golding, Robert B. O'Hara, Kirsten M. Parris, Peter A. Vesk, and Michael A. Mccarthy. Understanding co-occurrence by modelling species simultaneously with a Joint Species Distribution Model (JSDM). *Methods in Ecology and Evolution*, 5(5):397–406, 2014.

[29] R Core Team. *R: A Language and Environment for Statistical Computing*. R Foundation for Statistical Computing, Vienna, Austria, 2016.

[30] A. Rambaut, M.A. Suchard, D. Xie, and A.J. Drummond. Tracer v1.6. 2013.

[31] Patrick D. Schloss, Sarah L. Westcott, Thomas Ryabin, Justine R. Hall, Martin Hartmann, Emily B. Hollister, Ryan A. Lesniewski, Brian B. Oakley, Donovan H. Parks, Courtney J. Robinson, Jason W. Sahl, Blaz Stres, Gerhard G. Thallinger, David J. Van Horn, and Carolyn F. Weber. Introducing mothur: Open-source, platform-independent, community-supported software for describing and comparing microbial communities. *Applied and Environmental Microbiology*, 75(23):7537–7541, 2009.

[32] Susanne Schmitt, Peter Tsai, James Bell, Jane Fromont, Micha Ilan, Niels Lindquist, Thierry Perez, Allen Rodrigo, Peter J. Schupp, Jean Vacelet, Nicole Webster, Ute Hentschel, and Michael W. Taylor. Assessing the complex sponge microbiota: core, variable and species-specific bacterial communities in marine sponges. *The ISME Journal*, 6(3):564–576, 2012.

[33] Torsten Thomas, Lucas Moitinho-Silva, Miguel Lurgi, Johannes R Björk, Cole Easson, Carmen Astudillo-García, Julie B Olson, Patrick M Erwin, Susanna López-Legentil, Heidi Luter, et al. Diversity, structure and convergent evolution of the global sponge microbiome. *Nature Communications*, 7(11870), 2016.

bioRxiv preprint doi: https://doi.org/10.1101/137943; this version posted May 14, 2017. The copyright holder for this preprint (which was not certified by peer review) is the author/funder, who has granted bioRxiv a license to display the preprint in perpetuity. It is made available under aCC-BY-NC 4.0 International license.

[34] John N Thompson. *The coevolutionary process*. University of Chicago Press, 1994.

[35] Gleb Tikhonov, Nerea Abrego, David Dunson, and Otso Ovaskainen. Using joint species distribution models for evaluating how species-to-species associations depend on the environmental context. *Methods in Ecology and Evolution*, 8(4):443–452, 2017.

[36] Hirokazu Toju, Masato Yamamichi, Paulo R. Guimarães Jr, Jens M. Olesen, Akihiko Mougi, Takehito Yoshida, and John N. Thompson. Species-rich networks and eco-evolutionary synthesis at the metacommunity level. *Nature Ecology & Evolution*, 1:0024EP, Jan 2017.

[37] Jenny Tung, Luis B. Barreiro, Michael B. Burns, Jean-Christophe Grenier, Josh Lynch, Laura E. Grieneisen, Jeanne Altmann, Susan C. Alberts, Ran Blekhman, and Elizabeth A. Archie. Social networks predict gut microbiome composition in wild baboons. *eLife*, 4:e05224, 2015.

[38] Jean Vacelet and Claude Donadey. Electron microscope study of the association between some sponges and bacteria. *Journal of Experimental Marine Biology and Ecology*, 30(3):301–314, 1977.

[39] Mark Vellend. Conceptual Synthesis in Community Ecology. *The Quarterly Review of Biology*, 85(2):183–206, 2010.

[40] David I. Warton, F. Guillaume Blanchet, Robert B. O'Hara, Otso Ovaskainen, Sara Taskinen, Steven C. Walker, and Francis K. C. Hui. So Many Variables: Joint Modeling in Community Ecology. *Trends in Ecology and Evolution*, 30:1–14, 2015.

[41] David I. Warton, Stephen T. Wright, and Yi Wang. Distance-based multivariate analyses confound location and dispersion effects. *Methods in Ecology and Evolution*, 3(1):89–101, 2012.

[42] Nicole S. Webster, Michael W. Taylor, Faris Behnam, Sebastian Lücker, Thomas Rattei, Stephen Whalan, Matthias Horn, and Michael Wagner. Deep sequencing reveals exceptional diversity and modes of transmission for bacterial sponge symbionts. *Environmental Microbiology*, 12(8):2070–2082, 2010.

[43] Li C. Xia, Joshua A. Steele, Jacob A. Cram, Zoe G. Cardon, Sheri L. Simmons, Joseph J. Vallino, Jed A. Fuhrman, and Fengzhu Sun. Extended local similarity analysis (eLSA) of microbial community and other time series data with replicates. *BMC Systems Biology*, 5(Suppl 2):S15, 2011.

[44] Lizhen Xu, Andrew D. Paterson, and Wei Xu. Bayesian latent variable models for hierarchical clustered count outcomes with repeated measures in microbiome studies. *Genetic Epidemiology*, 41(3):221–232, 2017.

bioRxiv preprint doi: https://doi.org/10.1101/137943; this version posted May 14, 2017. The copyright holder for this preprint (which was not certified by peer review) is the author/funder, who has granted bioRxiv a license to display the preprint in perpetuity. It is made available under aCC-BY-NC 4.0 International license.

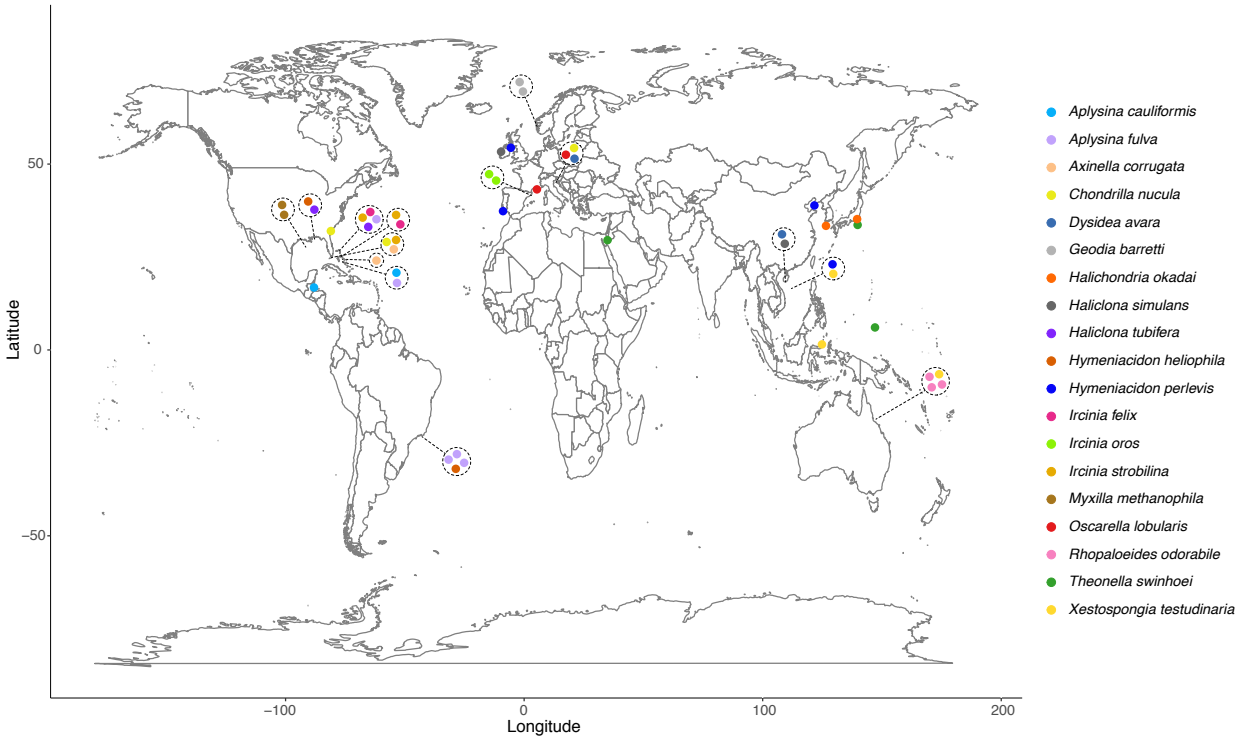

Figure 1: Overview of the broad spatial scale for which the data is distributed. Each point represents a collection site and each colour represents a host species. Note that some host species coexist within the same site. See Table S1 for more detailed information.

bioRxiv preprint doi: https://doi.org/10.1101/137943; this version posted May 14, 2017. The copyright holder for this preprint (which was not certified by peer review) is the author/funder, who has granted bioRxiv a license to display the preprint in perpetuity. It is made available under aCC-BY-NC 4.0 International license.

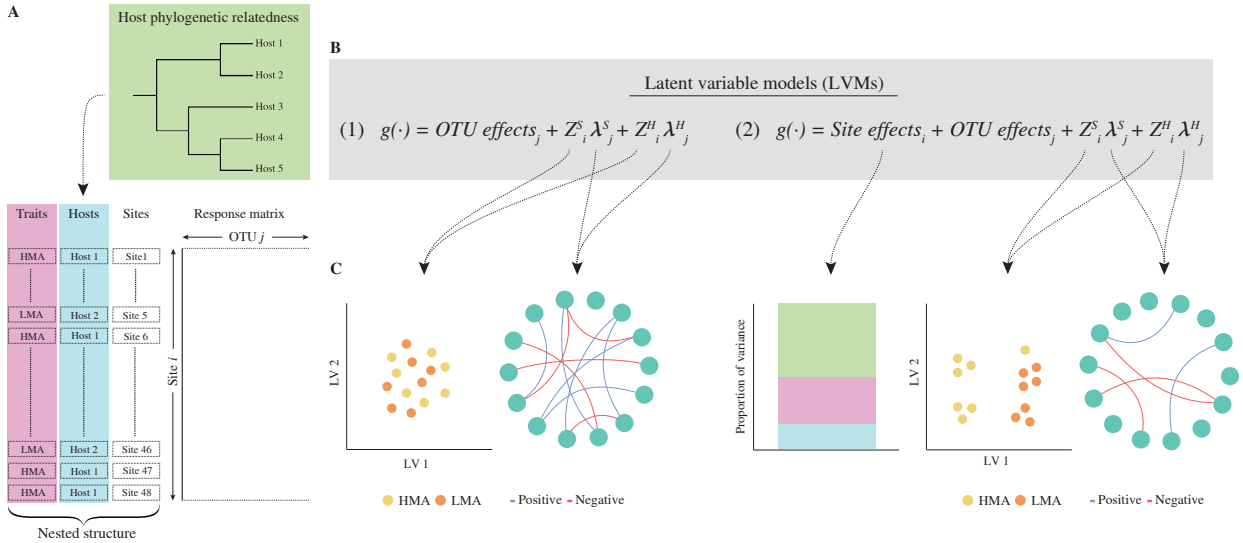

Figure 2: Conceptual figure of the modeling framework. Panel A shows a schematic figure of the response matrix. While columns correspond to OTUs, rows have a hierarchical structure where sites are nested within host species which are further nested within host traits (High Microbial Abundance (HMA) and Low Microbial Abundance (LMA)). At the host species level, the framework also accounts for phylogenetic relatedness. Panel B shows the two different joint species distribution models (JSDMs) with latent factors for site (S) and host species (H) level, each representing a different level of biological organization. The $g(\cdot)$ represents the different link function associated to the different response types. Panel C shows the corresponding output; because model (1) does not include site effects, its resulting ordination constructed from the latent factors are in terms of microbiota structure (i.e., a composite of abundance and composition), and because model (2) includes site effects, its resulting ordination constructed from the latent factors are in terms of microbiota composition only. The OTU-to-OTU association networks constructed from the corresponding factor loadings also differ for the two JSDM models. Note that ordinations and association networks are produced both on the site and host species level, respectively. Finally, as the site effects are nested within the host-specific features, model (2) partition variance in microbiota abundance or species richness into components directly reflecting the included host-specific features.

bioRxiv preprint doi: https://doi.org/10.1101/137943; this version posted May 14, 2017. The copyright holder for this preprint (which was not certified by peer review) is the author/funder, who has granted bioRxiv a license to display the preprint in perpetuity. It is made available under aCC-BY-NC 4.0 International license.

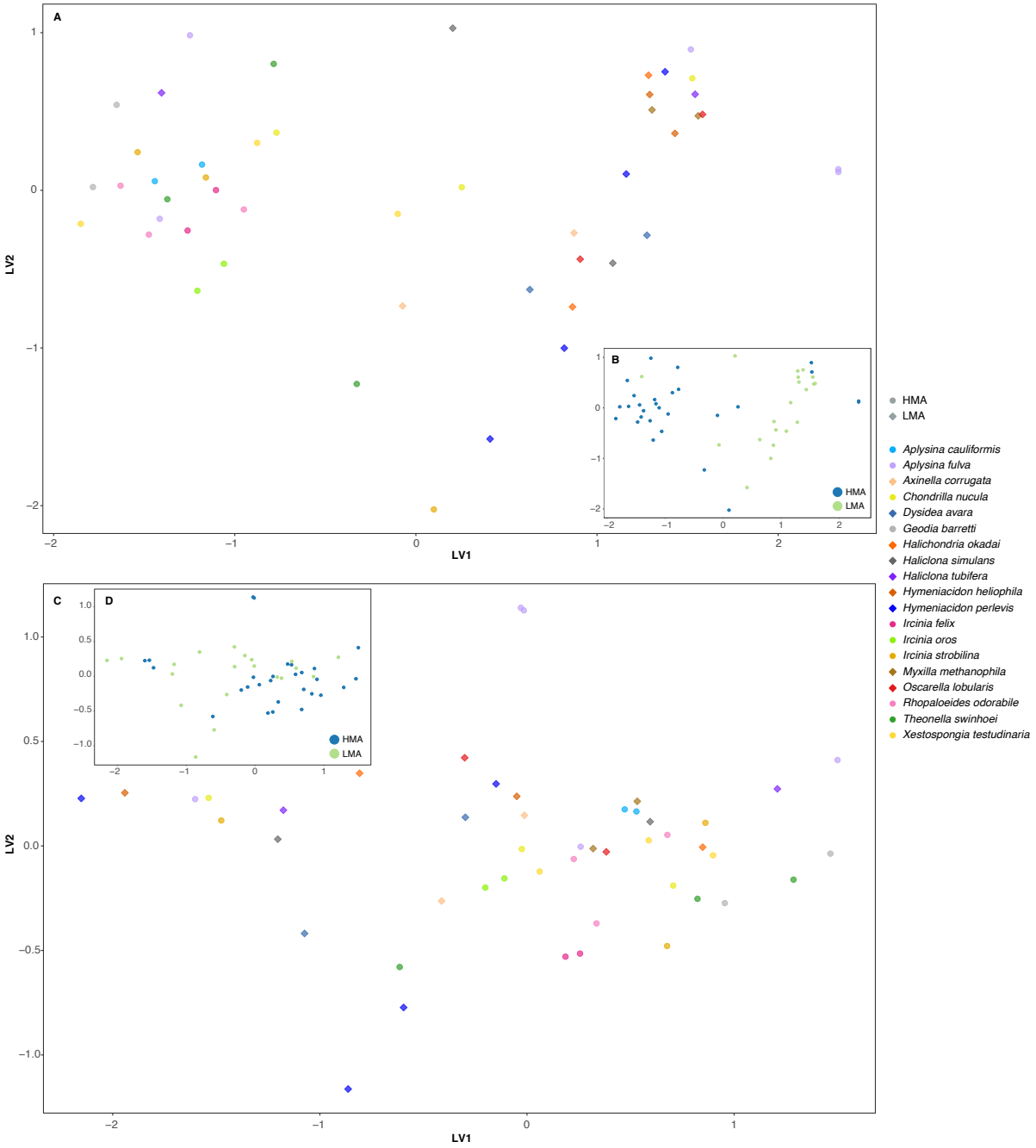

Figure 3: Model-based ordinations on the site level. Panel A and B show the model-based unconstrained ordination without site effects included. In panel A, sites are colored by host species and ecotype are depicted by different shapes (HMA=circles, LMA=diamonds), while in panel B sites are colored by ecotype only (HMA=blue, LMA=green). Panel C and D show the model-based unconstrained ordination with site effects included. In panel C, sites are colored by host species and ecotype is depicted by different shapes (HMA=circles, LMA=diamonds), while in panel D sites are colored by ecotype only (HMA=blue, LMA=green).

bioRxiv preprint doi: https://doi.org/10.1101/137943; this version posted May 14, 2017. The copyright holder for this preprint (which was not certified by peer review) is the author/funder, who has granted bioRxiv a license to display the preprint in perpetuity. It is made available under aCC-BY-NC 4.0 International license.

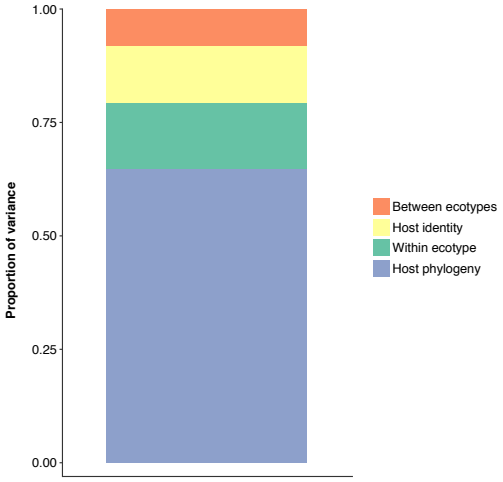

Figure 4: The proportion of variance in terms of total abundance among sites explained by the included host-specific features. Yellow corresponds to variance explained by host species identity, blue to host phylogenetic relatedness, green to variance within ecotypes, and finally red corresponds to variance explained by differences among the two ecotypes.

bioRxiv preprint doi: https://doi.org/10.1101/137943; this version posted May 14, 2017. The copyright holder for this preprint (which was not certified by peer review) is the author/funder, who has granted bioRxiv a license to display the preprint in perpetuity. It is made available under aCC-BY-NC 4.0 International license.

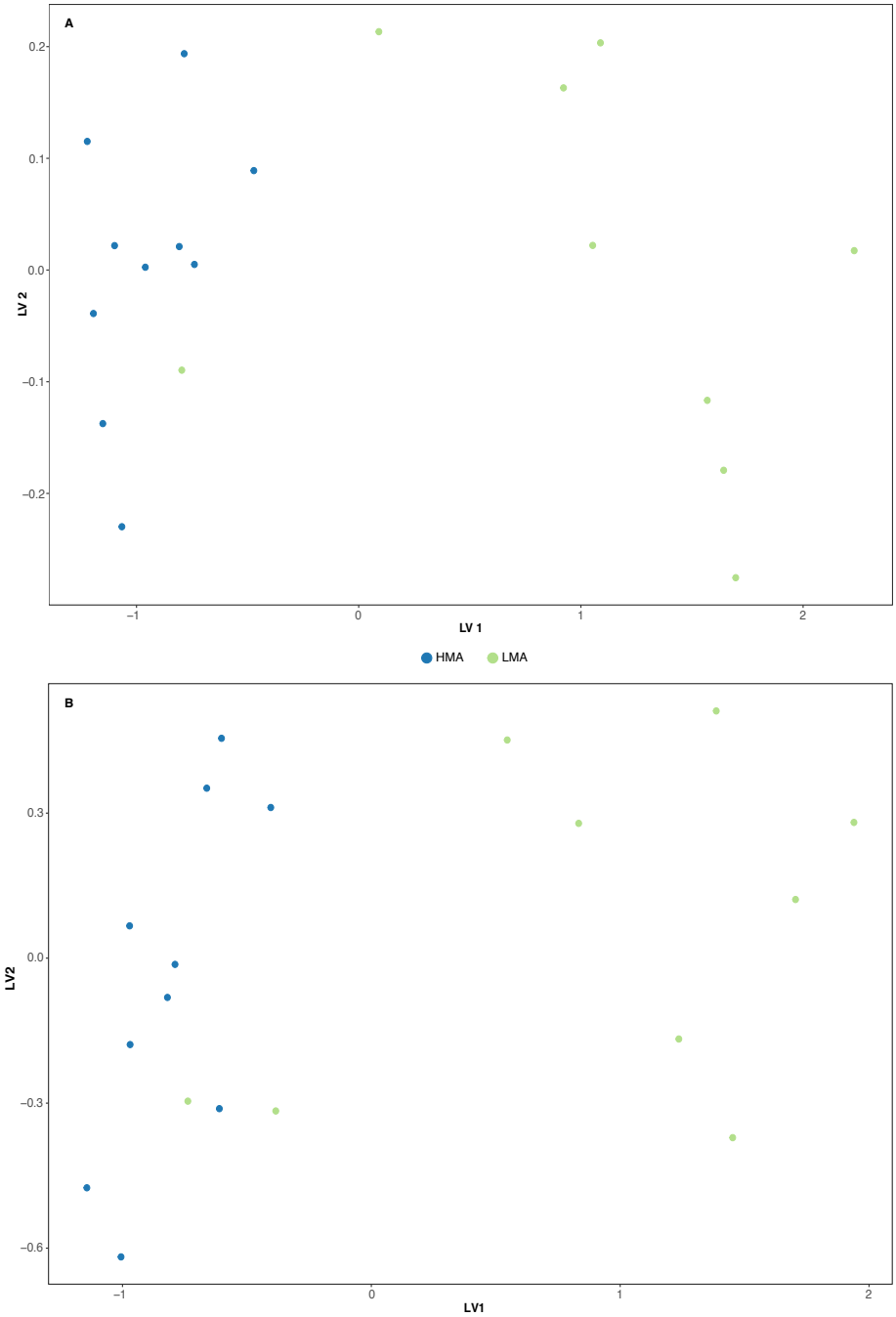

Figure 5: Model-based ordinations on the host species level. Panel A shows the model-based unconstrained ordination without site effects included, while panel B shows the model-based unconstrained ordination with site effects included. In both panels, host species are colored by ecotype (HMA=blue, LMA=green).

bioRxiv preprint doi: https://doi.org/10.1101/137943; this version posted May 14, 2017. The copyright holder for this preprint (which was not certified by peer review) is the author/funder, who has granted bioRxiv a license to display the preprint in perpetuity. It is made available under aCC-BY-NC 4.0 International license.

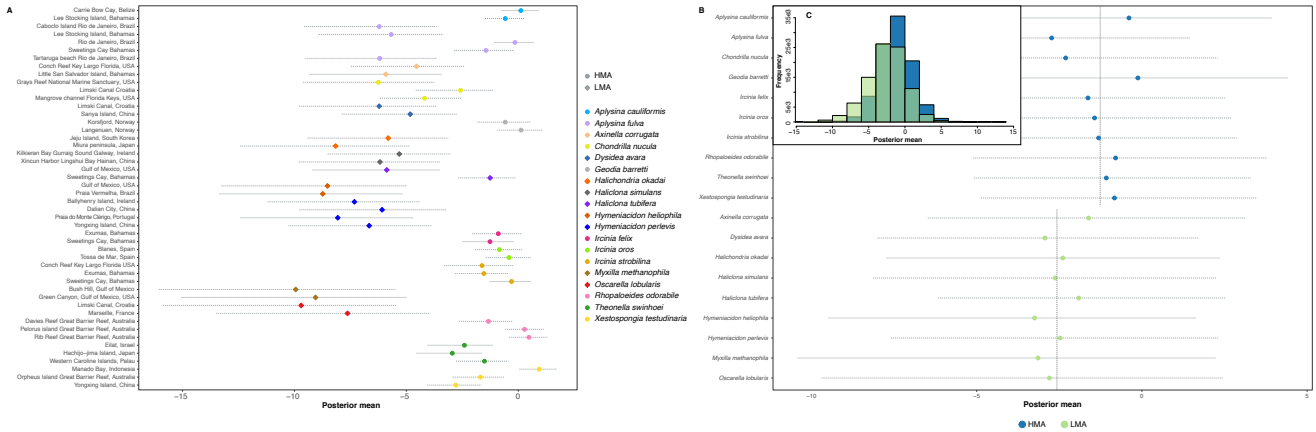

Figure 6: Caterpillar plots for differences in total abundance. Panel A shows a caterpillar plot for the parameter controlling the site effects, i.e., α_i. Each row correspond to a sites, colored by host species. The colored shape represent the posterior mean (± SD). The two ecotype are depicted by different shapes (HMA=circles, LMA=diamonds). Panel B shows a caterpillar plot for α_i's mean parameter, i.e., the $\mu(\text{host})_{s[r]}$. Rows correspond to host species colored by ecotype (HMA=blue, LMA=green). The vertical dashed lines correspond to the grand mean of each ecotype. Panel C shows the posterior probability distribution of $\mu(\text{host})_{s[r]}$ for HMA (blue) and LMA (green), respectively.

bioRxiv preprint doi: https://doi.org/10.1101/137943; this version posted May 14, 2017. The copyright holder for this preprint (which was not certified by peer review) is the author/funder, who has granted bioRxiv a license to display the preprint in perpetuity. It is made available under aCC-BY-NC 4.0 International license.

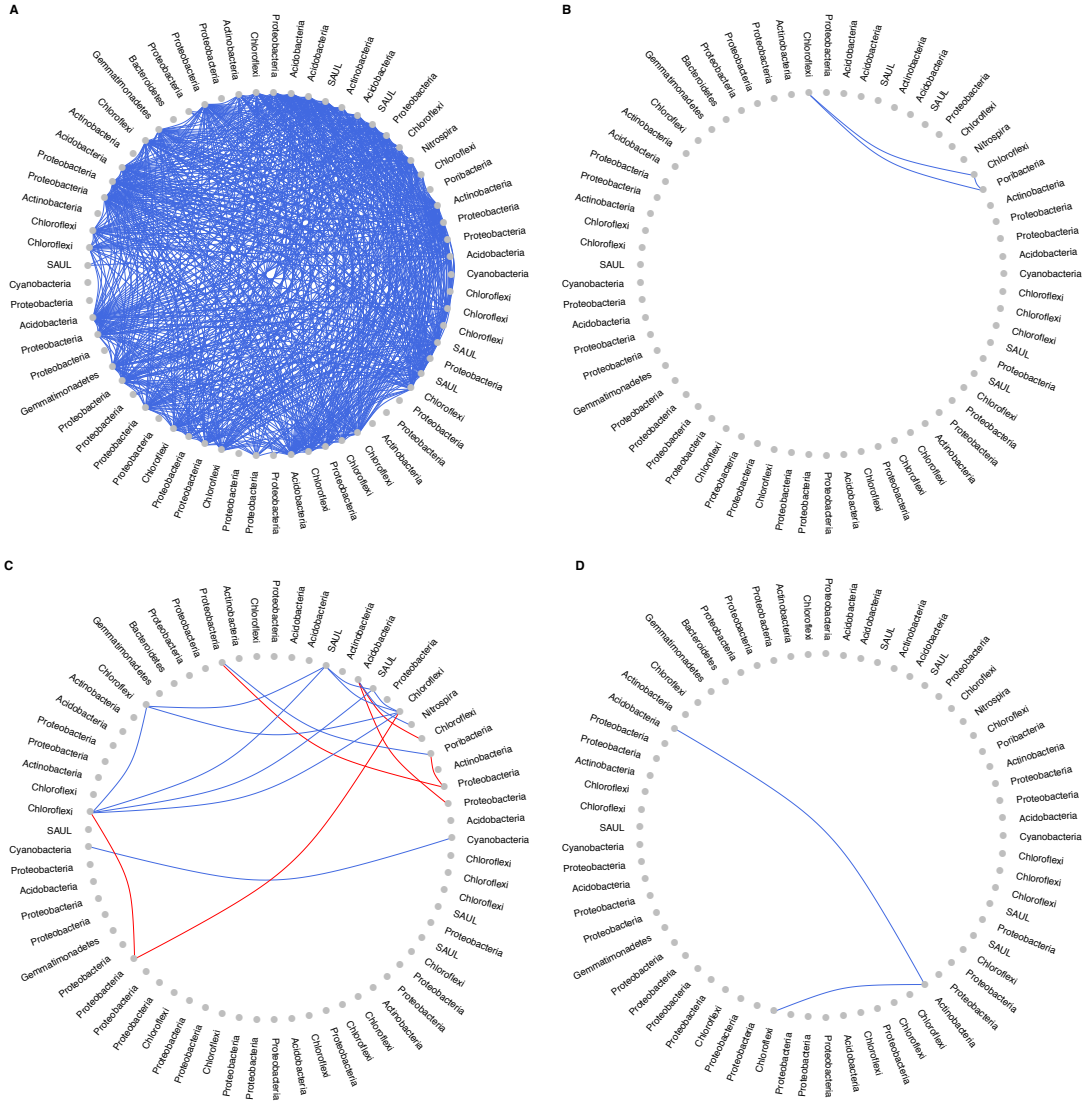

Figure 7: OTU-to-OTU association networks. Nodes represent OTUs with assigned taxonomy at the phylum-level, and links correspond to abundance correlations with at least 95% posterior probability. The top panel (A & B) shows networks generated from the model without site effects, thus correlations between OTUs are induced by both site and host-specific features as well as OTU-specific effects. The bottom panel (C & D) shows networks generated from the model with site effects included, thus correlations between OTUs are only OTU-specific effects. Panel A & C shows the association network for the site level and panel B & D shows the network for the host species level.

bioRxiv preprint doi: https://doi.org/10.1101/137943; this version posted May 14, 2017. The copyright holder for this preprint (which was not certified by peer review) is the author/funder, who has granted bioRxiv a license to display the preprint in perpetuity. It is made available under aCC-BY-NC 4.0 International license.

Supplementary Material

Table S1: Detailed information about the geographic location for each host species. The table shows each host species with its corresponding ecotype, sample site, ocean basin, and latitude and longitude.

Host species	Ecotype	Site	Ocean	Lat	Lon
Aplysina cauliformis	HMA	Carrie Bow Cay, Belize	Caribbean Sea	16.803	-88.082
Aplysina cauliformis	HMA	Lee Stocking Island, Bahamas	North Atlantic Ocean	23.769	-76.099
Aplysina fulva	HMA	Caboclo Island, Rio de Janeiro, Brazil	South Atlantic Ocean	-22.755	-41.890
Aplysina fulva	HMA	Lee Stocking Island, Bahamas	North Atlantic Ocean	23.769	-76.099
Aplysina fulva	HMA	Rio de Janeiro, Brazil	South Atlantic Ocean	-22.875	-43.278
Aplysina fulva	HMA	Sweetings Cay, Bahamas	North Atlantic Ocean	26.600	-77.900
Aplysina fulva	HMA	Tartaruga beach, Rio de Janeiro, Brazil	South Atlantic Ocean	-22.756	-41.904
Axinella corrugata	LMA	Conch Reef, Key Largo, Florida, USA	Caribbean Sea	24.950	-80.454
Axinella corrugata	LMA	Little San Salvador Island, Bahamas	North Atlantic Ocean	24.548	-75.934
Chondrilla nucula	HMA	Grays Reef, USA	North Atlantic Ocean	31.984	-81.019
Chondrilla nucula	HMA	Limski Canal, Croatia	Adriatic Sea	45.131	13.663
Chondrilla nucula	HMA	Mangrove channel, Florida Keys, USA	North Atlantic Ocean	24.863	-80.717
Dysidea avara	LMA	Limski Canal, Croatia	Adriatic Sea	45.131	13.663
Dysidea avara	LMA	Sanya Island, China	South China Sea	18.233	109.489
Geodia barretti	HMA	Korsfjord, Norway	North Atlantic Ocean	60.153	5.148
Geodia barretti	HMA	Langenuen, Norway	North Atlantic Ocean	59.978	5.382
Halichondria okadai	LMA	Jeju Island, South Korea	East China Sea	33.390	126.540
Halichondria okadai	LMA	Miura peninsula, Japan	Pacific Ocean	35.199	139.586
Haliclona simulans	LMA	Galway, Ireland	North Atlantic Ocean	53.316	-9.669
Haliclona simulans	LMA	Sanya Island, China	South China Sea	18.402	109.994
Haliclona tubifera	LMA	Gulf of Mexico, USA	Gulf of Mexico	30.138	-88.002
Haliclona tubifera	LMA	Sweetings Cay, Bahamas	North Atlantic Ocean	26.600	-77.900
Hymeniacidon heliophila	LMA	Gulf of Mexico, USA	Gulf of Mexico	30.138	-88.002
Hymeniacidon heliophila	LMA	Praia Vermelha, Brazil	South Atlantic Ocean	-22.955	-43.163
Hymeniacidon perlevis	LMA	Ballyhenry Island, Ireland	North Atlantic Ocean	54.393	-5.575
Hymeniacidon perlevis	LMA	Dalian City, China	Yellow Sea	38.867	121.683
Hymeniacidon perlevis	LMA	Praia de Monte Clerigo, Portugal	North Atlantic Ocean	37.342	-8.852
Hymeniacidon perlevis	LMA	Yongxing Island, China	South China Sea	16.600	112.200
Ircinia felix	HMA	Exumas, Bahamas	North Atlantic Ocean	24.881	-76.792
Ircinia felix	HMA	Sweetings Cay, Bahamas	North Atlantic Ocean	26.560	-77.884
Ircinia oros	HMA	Blanes, Spain	Mediterranean Sea	41.673	2.804
Ircinia oros	HMA	Tossa de Mar, Spain	Mediterranean Sea	41.720	2.941
Ircinia strobilina	HMA	Conch Reef, Key Largo, Florida USA	Caribbean Sea	24.950	-80.454
Ircinia strobilina	HMA	Exumas, Bahamas	North Atlantic Ocean	24.881	-76.792
Ircinia strobilina	HMA	Sweetings Cay, Bahamas	North Atlantic Ocean	26.600	-77.900
Myxilla methanophila	LMA	Bush Hill, USA	Gulf of Mexico	27.783	-91.507
Myxilla methanophila	LMA	Green Canyon, USA	Gulf of Mexico	27.740	-91.222
Oscarella lobularis	LMA	Limski Canal, Croatia	Adriatic Sea	45.131	13.663
Oscarella lobularis	LMA	Marseille, France	Mediterranean Sea	43.197	5.364
Rhopaloeides odorabile	HMA	Davies Reef, Australia	Coral Sea	-18.826	147.641
Rhopaloeides odorabile	HMA	Pelorus island, Australia	Coral Sea	-18.545	146.488
Rhopaloeides odorabile	HMA	Rib Reef, Australia	Coral Sea	-18.492	146.878
Theonella swinhoei	HMA	Eilat, Israel	Red Sea	29.531	34.957
Theonella swinhoei	HMA	Hachijo-jima Island, Japan	Pacific Ocean	33.633	139.800
Theonella swinhoei	HMA	Western Caroline Islands, Palau	Pacific Ocean	6.050	147.083
Xestospongia testudinaria	HMA	Manado Bay, Indonesia	Celebes Sea	1.486	124.835
Xestospongia testudinaria	HMA	Orpheus Island, Australia	Coral Sea	-18.560	146.485
Xestospongia testudinaria	HMA	Yongxing Island, China	South China Sea	16.833	112.333

bioRxiv preprint doi: https://doi.org/10.1101/137943; this version posted May 14, 2017. The copyright holder for this preprint (which was not certified by peer review) is the author/funder, who has granted bioRxiv a license to display the preprint in perpetuity. It is made available under aCC-BY-NC 4.0 International license.

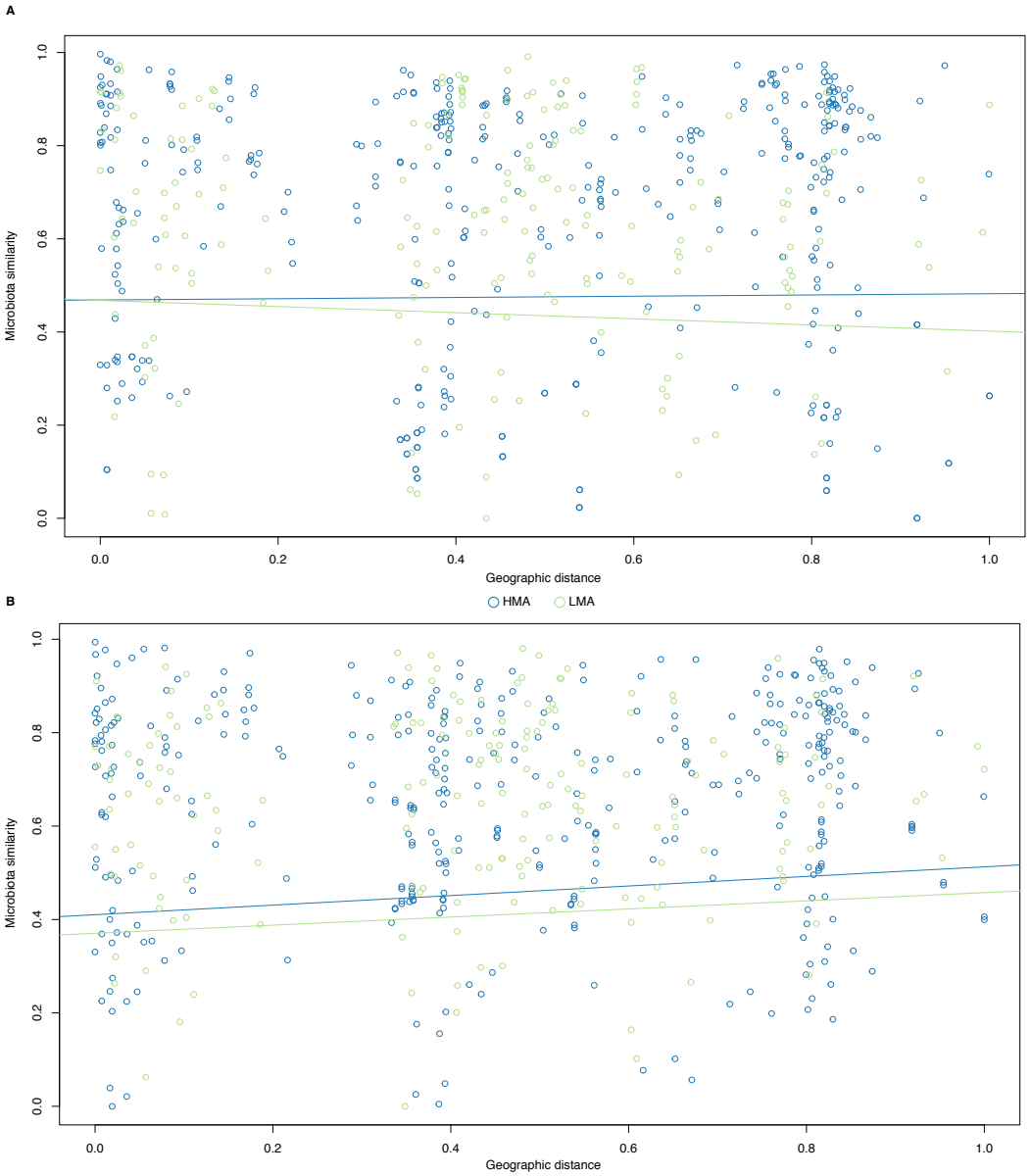

Figure S1: Distance-decay relationships for the NB models. The y-axis shows community similarity and the x-axis geographic distance. While panel A shows the relationship for the model without controlling for site effects, panel B shows the relationship when adjusting for site effects. Sites with HMA hosts are colored blue and sites with LMA hosts are colored green. In panel A, the slopes are: HMA=0.01113 and LMA=-0.06062. In panel B, the slopes are: HMA=0.0580 and LMA=0.05392.

Probit model

Below follows the specification of the probit models, as well as the plots generated from these models.

bioRxiv preprint doi: https://doi.org/10.1101/137943; this version posted May 14, 2017. The copyright holder for this preprint (which was not certified by peer review) is the author/funder, who has granted bioRxiv a license to display the preprint in perpetuity. It is made available under aCC-BY-NC 4.0 International license.

Probit model specification: Let $\mathcal{N}(\mu, \sigma^2)$ denote a normal distribution with mean μ and variance σ^2, and analogously, let $\mathcal{MVN}(\boldsymbol{\mu}, \Sigma)$ denote a multivariate normal distribution with mean vector and covariance matrix Σ.

To define the model, we denote sites by the index $i = 1, \ldots, m$ and the OTUs by index $j = 1, \ldots, n$, where m is the total number of sites and n is the total number of OTUs. The rows of the response matrix have a hierarchical structure typical for many microbiota data. Specifically, the $m = 48$ sites are nested within the $s = 19$ host species, with the 19 host species nested within one of $r = 2$ ecotypes (Figure 2). We denote the response matrix by y_{ij}, so that $y_{ij} = 1$ if OTU j is harbored by individual i and otherwise $y_{ij} = 0$. We model OTU occurrences with a probit regression, implemented as $y_{ij} = 1_{z_{ij}>0}$, where the latent liability z_{ij} is defined as

$$\boldsymbol{z}_i = \alpha_i + \beta_j + \sum_{q=1}^{2} Z^S_{iq}\lambda^S_{qj} + \sum_{q=1}^{2} Z^H_{s[i]q}\lambda^H_{qj}; \quad i = 1, \ldots, 48; \quad j = 1, \ldots, 65; \quad q = 1, \ldots, 2 \tag{S1}$$

$$\begin{aligned}
\beta_j &\sim Cauchy(0, 2.5) \\
\alpha_i &\sim \mathcal{N}(\mu_i, \sigma^2(\text{host})) \\
\mu_i &= \mu(\text{host})_{s[r]} + \tau * \mu(\text{phylo})_s; \quad r = 1, 2;\ s = 1, \ldots, 19 \\
\mu(\text{host})_{s[r]} &\sim \mathcal{N}(\mu(\text{ecotype})_r, \sigma^2(\text{ecotype})) \\
\mu(\text{ecotype})_r &\sim Cauchy(0, 2.5) \\
\boldsymbol{\mu}(\text{phylo})_s &\sim \mathcal{MVN}(\mathbf{0}, \Sigma(\text{phylo}))
\end{aligned} \tag{S2}$$

For the model without site effects α_i included, its associated nested structure were removed from Equation S1, such that $\boldsymbol{z}_i = \beta_j + \sum_{q=1}^{2} Z^S_{iq}\lambda^S_{qj} + \sum_{q=1}^{2} Z^H_{s[i]q}\lambda^H_{qj}$. Please see section Joint species distribution models in the main text for further information regarding parameter definitions and priors.

bioRxiv preprint doi: https://doi.org/10.1101/137943; this version posted May 14, 2017. The copyright holder for this preprint (which was not certified by peer review) is the author/funder, who has granted bioRxiv a license to display the preprint in perpetuity. It is made available under aCC-BY-NC 4.0 International license.

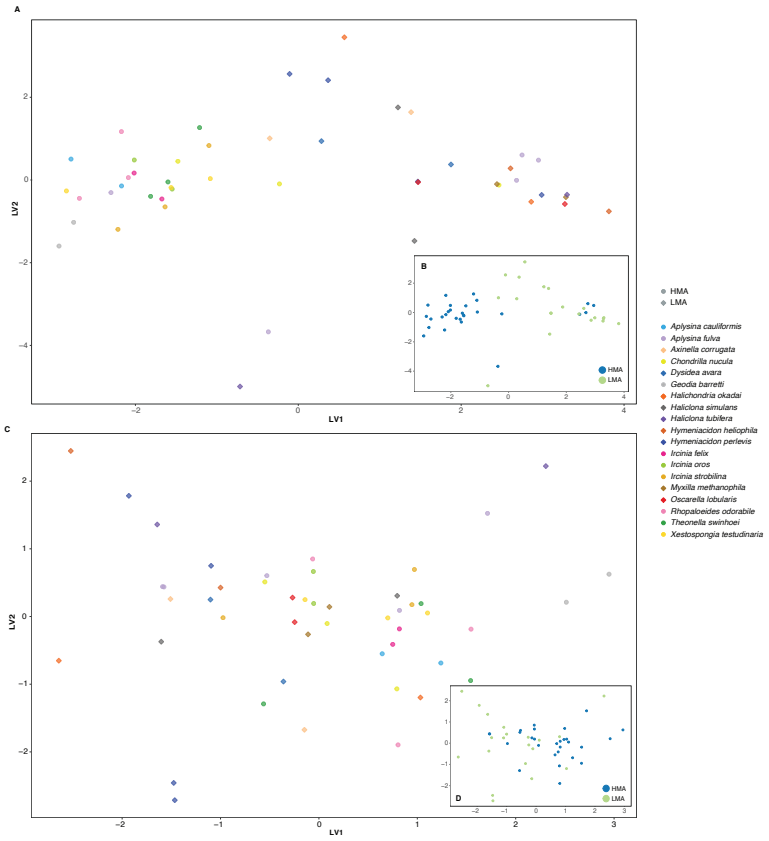

Figure S2: Model-based ordinations on the site level. Panel A and B show the model-based unconstrained ordination without site effects included. In panel A, sites are colored by host species and ecotype are depicted by different shapes (HMA=circles, LMA=diamonds), while in panel B sites are colored by ecotype only (HMA=blue, LMA=green). Panel C and D show the model-based unconstrained ordination with site effects included. In panel C, sites are colored by host species and ecotype is depicted by different shapes (HMA=circles, LMA=diamonds), while in panel D sites are colored by ecotype only (HMA=blue, LMA=green).

bioRxiv preprint doi: https://doi.org/10.1101/137943; this version posted May 14, 2017. The copyright holder for this preprint (which was not certified by peer review) is the author/funder, who has granted bioRxiv a license to display the preprint in perpetuity. It is made available under aCC-BY-NC 4.0 International license.

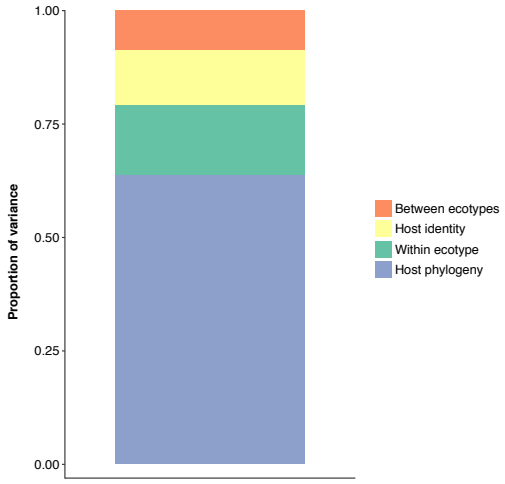

Figure S3: The proportion of variance in terms of total abundance among sites explained by the included host-specific features. Yellow corresponds to variance explained by host species identity, blue to host phylogenetic relatedness, green to variance within ecotypes, and finally red corresponds to variance explained by differences among the two ecotypes.

bioRxiv preprint doi: https://doi.org/10.1101/137943; this version posted May 14, 2017. The copyright holder for this preprint (which was not certified by peer review) is the author/funder, who has granted bioRxiv a license to display the preprint in perpetuity. It is made available under aCC-BY-NC 4.0 International license.

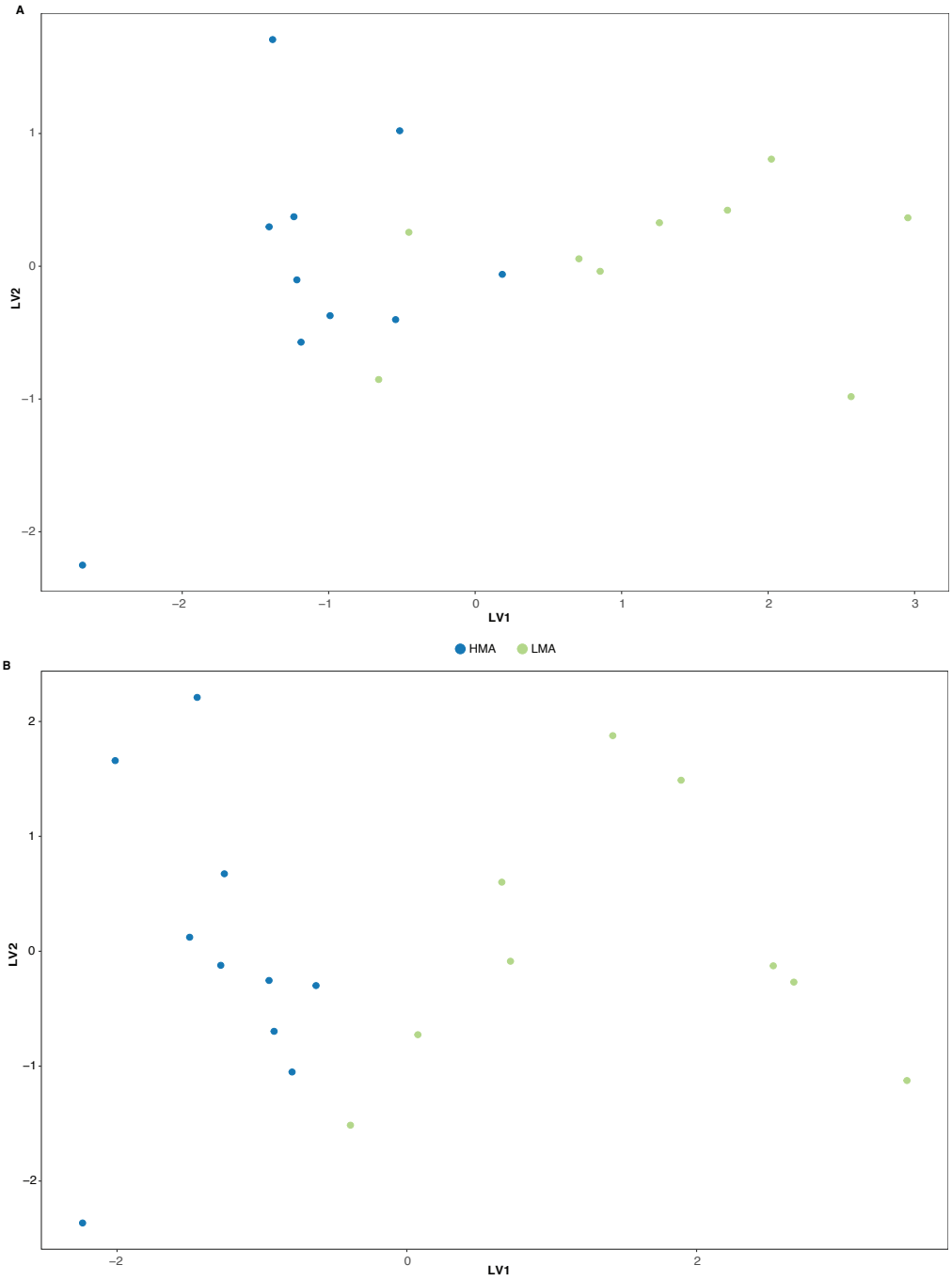

Figure S4: Model-based ordinations on the host species level. Panel A shows the model-based unconstrained ordination without site effects included, while panel B shows the model-based unconstrained ordination with site effects included. In both panels, host species are colored by ecotype (HMA=blue, LMA=green).

bioRxiv preprint doi: https://doi.org/10.1101/137943; this version posted May 14, 2017. The copyright holder for this preprint (which was not certified by peer review) is the author/funder, who has granted bioRxiv a license to display the preprint in perpetuity. It is made available under aCC-BY-NC 4.0 International license.

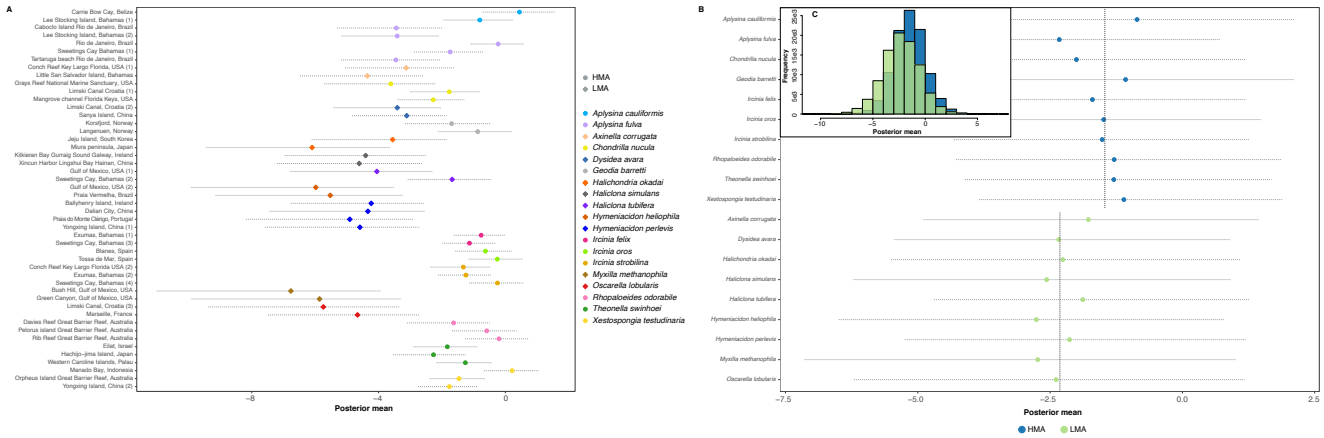

Figure S5: Caterpillar plots for differences in total abundance. Panel A shows a caterpillar plot for the parameter controlling the site effects, i.e., α_i. Each row correspond to a sites, colored by host species. The colored shape represent the posterior mean (± SD). The two ecotype are depicted by different shapes (HMA=circles, LMA=diamonds). Panel B shows a caterpillar plot for α_i's mean parameter, i.e., the $\mu(\text{host})_{s[r]}$. Rows correspond to host species colored by ecotype (HMA=blue, LMA=green). The vertical dashed lines correspond to the grand mean of each ecotype. Panel C shows the posterior probability distribution of $\mu(\text{host})_{s[r]}$ for HMA (blue) and LMA (green), respectively.

bioRxiv preprint doi: https://doi.org/10.1101/137943; this version posted May 14, 2017. The copyright holder for this preprint (which was not certified by peer review) is the author/funder, who has granted bioRxiv a license to display the preprint in perpetuity. It is made available under aCC-BY-NC 4.0 International license.

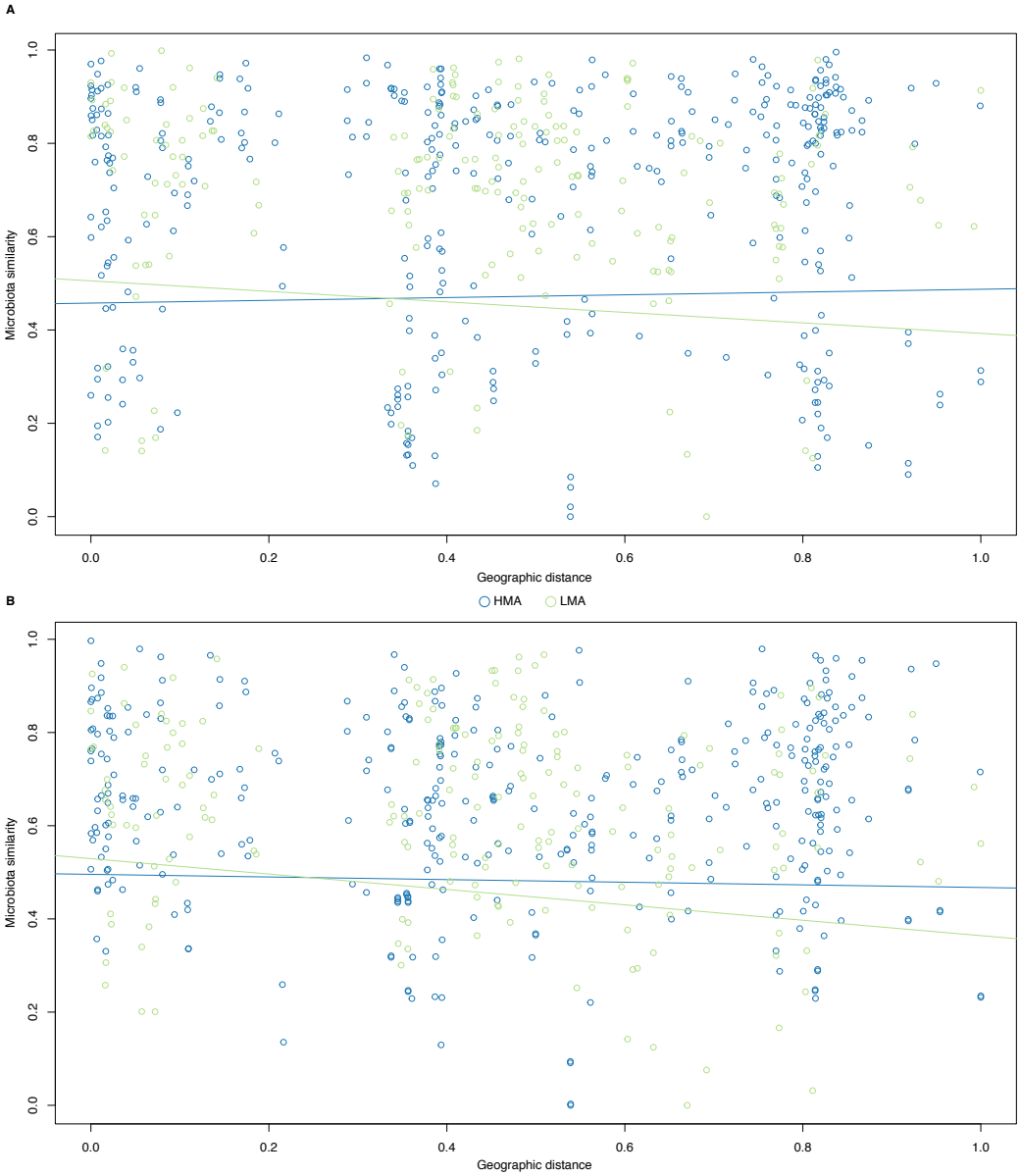

Figure S6: Distance-decay relationships. The y-axis shows community similarity and the x-axis geographic distance. While panel A shows the relationship for the model without controlling for site effects, panel B shows the relationship when adjusting for site effects. Sites with HMA hosts are colored blue and sites with LMA hosts are colored green. In panel A, the slopes are: HMA=0.02259 and LMA=-0.07438. In panel B, the slopes are: HMA=-0.01198 and LMA=-0.1038.

bioRxiv preprint doi: https://doi.org/10.1101/137943; this version posted May 14, 2017. The copyright holder for this preprint (which was not certified by peer review) is the author/funder, who has granted bioRxiv a license to display the preprint in perpetuity. It is made available under aCC-BY-NC 4.0 International license.

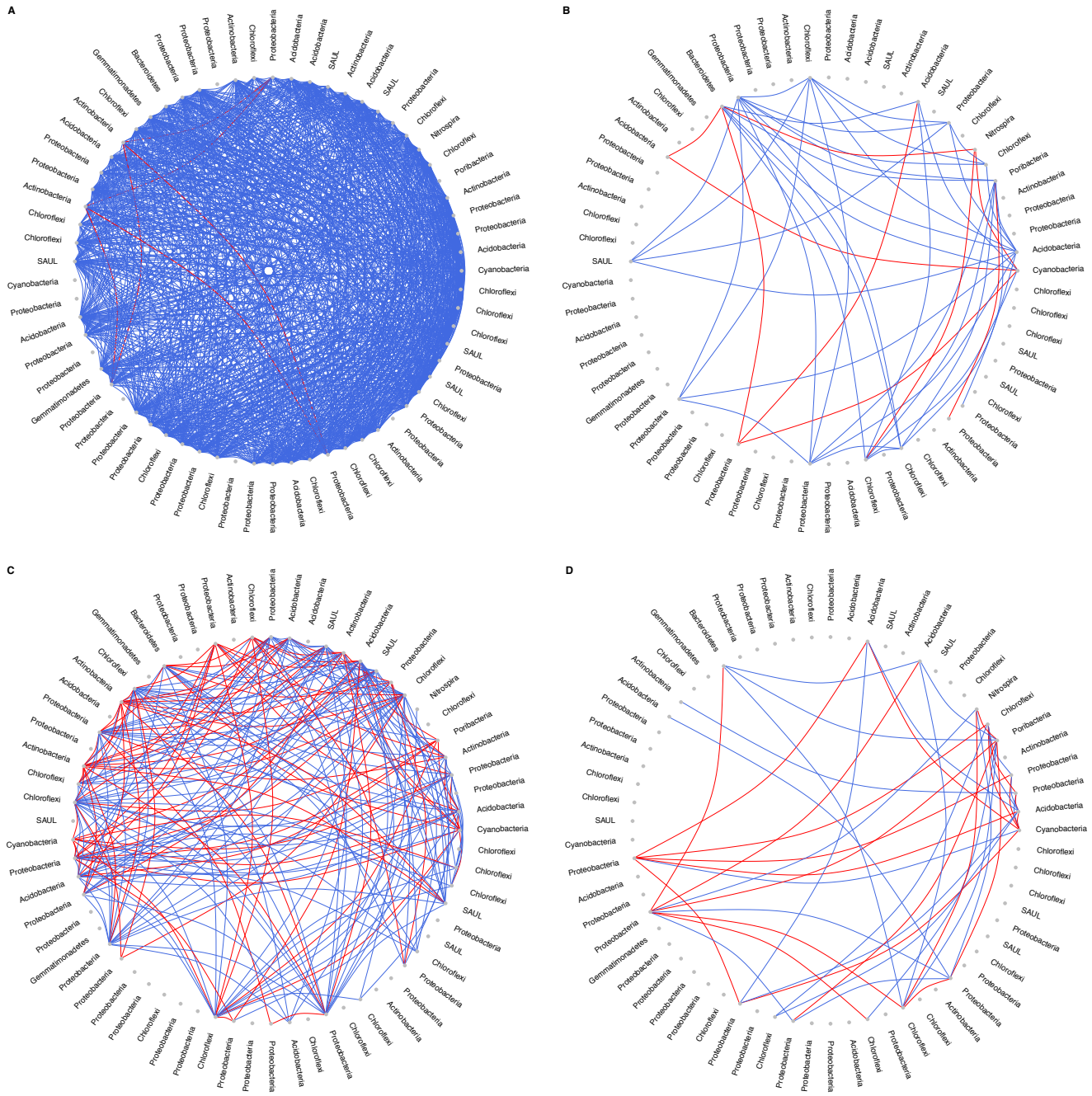

Figure S7: OTU-to-OTU association networks. Nodes represent OTUs with assigned taxonomy at the phylum-level, and links correspond to co-occurrences with at least 95% posterior probability. The top panel (A & B) shows networks generated from the model without site effects, thus correlations between OTUs are induced by both site and host-specific features as well as OTU-specific effects. The bottom panel (C & D) shows networks generated from the model with site effects included, thus correlations between OTUs are only OTU-specific effects. Panel A & C show the association network for the site level and panel B & D shows the network for the host species level.